A positional FEM formulation applied to 2D dynamic nonlinear analysis of structures and mechanisms with improved frictional internal sliding connections

***Tiago Morkis Siqueira[1] and Humberto Breves Coda[1]**

[1]Department of Structural Engineering, São Carlos School of Engineering, University of São Paulo, São Carlos, SP, Brazil.

*Presenting and corresponding author: morkis@usp.br

Abstract

In this work we extend a total Lagrangian formulation applied to the dynamical analysis of plane frames containing sliding connections (prismatic and cylindrical joints) to include frictional dissipation. An improvement in the friction force model is proposed to smooth the force transition from rest to motion states, allowing the proper modelling of residual displacements at the joints. Friction dissipation is added to the total mechanical energy for the achievement of the equations of motion by the Principle of Stationary Total Energy. The resulting nonlinear equations are solved by the Newton-Raphson method. Some examples are presented to show the formulation effectiveness.

Keywords: Friction model; Sliding connection; Nonlinear dynamics; Lagrange multiplier.

Introduction

In the dynamical analysis of structures and mechanisms conservative systems simplifications are frequently assumed. However, real bodies present dissipation due to several sources. The frictional dissipation effect, in particular, is important to be considered when relative motion from parts of the body exists. This is the case of sliding connections, such as prismatic and cylindrical joints, that by introducing translational movement among body members allows friction forces to develop along their surfaces contact.

The friction phenomena itself has a very complex nature that mathematical models try to describe, with more or less accuracy, depending on which aspects of the friction force the proposed expressions intent to consider. The models become more detailed and representative at the cost of more parameters. A comprehensive surveys on friction models can be found in [1–3]. In the literature, friction models can be classified generally in dynamic or static [3], whether the force is, respectively, time dependent or not. Thus, static models, as opposed to dynamical models, dismiss the introduction of state variables to the problem, rendering a straightforward description of the force expression. Still, static models have difficulties in describing the discontinuity of the friction force at null speed, which results in instabilities in the numerical solution. Several models try to circumvent this problem [4–9] commonly assuming null friction at null speed, which is not a good approximation when relative motion is intermittent, or require additional parameters for the transition between motion and rest states.

In this work, we propose a modification on a classic static friction model to be employed in sliding connections of plane frame finite elements by positional formulation. The improved model is based on the Coulomb friction considering the Stribeck curve and viscous effect. To reduce the abrupt transition between rest and motion states, an interpolation of the static friction value to the resultant force is employed in a quasi-null relative speed interval. Thus, the proposed model intents to represent the force transition in a smooth way, allowing the description of residual displacements when the final stop stage is achieved, which is important to ensure high precision movements reproduction in structures and mechanisms.

The framework used to model the dynamical system [10,11] is a fully nonlinear finite element approach for large deformations based on a total Lagrangian description of the solids which uses positions as the main degrees of freedom. The Saint-Venant-Kirchhoff constitutive model is adopted to define the plane frame elastic strain energy using the Green-Lagrange strain and the second Piola-Kirchhoff stress tensor. Since in this technique velocity and acceleration are referred to a Lagrangian inertial reference frame, the Newmark approximation is applied to integrate time. The sliding connections, as prismatic and cylindrical joints, are introduced in the total energy of the system by means of Lagrange multipliers [11]. Moreover, friction dissipation is added to the energy expression to allow finding the equations of motion (comprising the frictional effect) by the Principle of Stationary Total Energy. The resulting nonlinear system is solved by the Newton-Raphson method.

This work is organized as follows. First brief aspects of the nonlinear plane frame element need to be presented followed by the kinematical constraints that the sliding connections impose. Then, the dynamical equilibrium is obtained. Known the system parameters, the friction force can be introduced in its variational form and the improved model is presented. Time integration and system solution follows this explanation. Lastly, examples are shown to demonstrate the developed formulation. Dyadic notation is preferred throughout this text due its brevity; however, index notation is also used to clarify particular aspects when necessary.

Nonlinear finite element kinematics

The plane frame finite element employed is presented thoroughly elsewhere [10,11], however, to develop the present work some aspects need to be briefly stated. As the finite element behaviour is represented by a total Lagrangian description, its strain field needs to be obtained as a function of the initial and current configurations of the solid, restricted to a finite number of degrees of freedom.

In the positional approach of the FEM, instead of nodal displacements, the parameters of the discretized plane frame are its positions (coordinates) and the cross section angle (Fig. 1). The deformation function, $\vec{f}$, depicted in Fig. 2, can be written indirectly as function of the non-dimensional space and nodal parameters by mappings from the non-dimensional space to the initial configuration, $\vec{f}^{\,0}$, as:

$$
\begin{aligned}
f_1^0 &= x_1 = \phi_\ell(\xi) X_1^\ell + \frac{h_0}{2}\eta\cos\left[\phi_\ell(\xi)\theta_\ell^0\right] \\
f_2^0 &= x_2 = \phi_\ell(\xi) X_2^\ell + \frac{h_0}{2}\eta\sin\left[\phi_\ell(\xi)\theta_\ell^0\right]
\end{aligned}
\tag{1}
$$

and to the current configuration, $\vec{f}^{\,1}$, as:

$$
\begin{aligned}
f_1^1 = y_1 &= \phi_\ell(\xi) Y_1^\ell + \frac{h_0}{2}\eta \cos[\phi_\ell(\xi)\theta_\ell] \\
f_2^1 = y_2 &= \phi_\ell(\xi) Y_2^\ell + \frac{h_0}{2}\eta \sin[\phi_\ell(\xi)\theta_\ell]
\end{aligned}
\tag{2}
$$

where $\vec{x}$ and $\vec{y}$ represents any point on the domain of a finite element in the initial and current configuration, respectively. The coordinates for both directions $i = 1,2$ of each node ℓ along the reference line in the initial and current configurations are X_i^ℓ and Y_i^ℓ, respectively. The initial nodal value of the cross section angle is θ_ℓ^0 and after deformation is denoted as θ_ℓ. In addition, the cross section height is h_0, ξ is the non-dimensional space variable in the direction of the reference line and η follows the height direction. The shape functions $\phi_\ell(\xi)$ are obtained by Lagrange polynomials of any order.

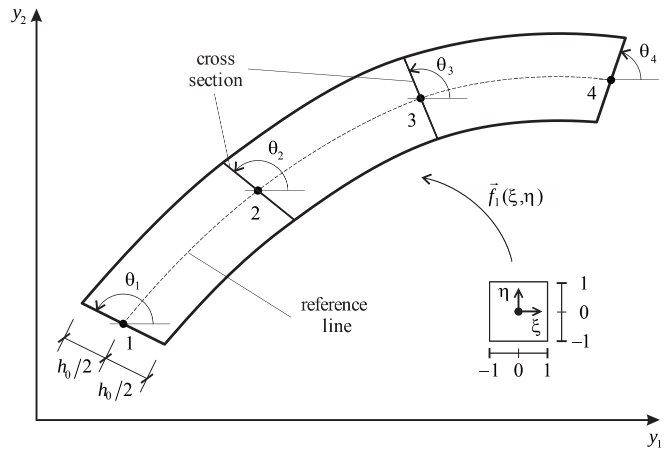

Fig. 1. Current configuration mapping for a cubic approximation

The deformation function can be written as a composition of the previous mappings, eq. (1) and (2), as presented by [12,13], as:

$$\vec{f} = \vec{f}^{\,1} \circ (\vec{f}^{\,0})^{-1} \tag{3}$$

Since only the gradient $\mathbf{A}$ of the deformation function, but not the function itself, is necessary to obtain the strain field [14], we can write:

$$\mathbf{A} = Grad(\vec{f}) = \mathbf{A}^1 . (\mathbf{A}^0)^{-1} \tag{4}$$

where,

$$A_{ij}^0 = \frac{\partial f_i^0}{\partial \xi_j} \qquad \text{and} \qquad A_{ij}^1 = \frac{\partial f_i^1}{\partial \xi_j} \tag{5}$$

During the iterative solution strategy both $\mathbf{A}^0$ and $\mathbf{A}^1$ are numerical values calculated at the integration points resulting in a purely numerical procedure.

Since the Saint-Venant-Kirchhoff constitutive law is employed, the Green-Lagrange strain tensor $\mathbf{E}$ have to be calculated. This objective measure is given, for instance, by [14]:

$$\mathbf{E} = \frac{1}{2}(\mathbf{C} - \mathbf{I}) = \frac{1}{2}(\mathbf{A}^t \cdot \mathbf{A} - \mathbf{I}) \tag{6}$$

where $\mathbf{I}$ is the second order identity tensor and $\mathbf{C} = \mathbf{A}^t \cdot \mathbf{A}$ is the right Cauchy-Green stretch tensor.

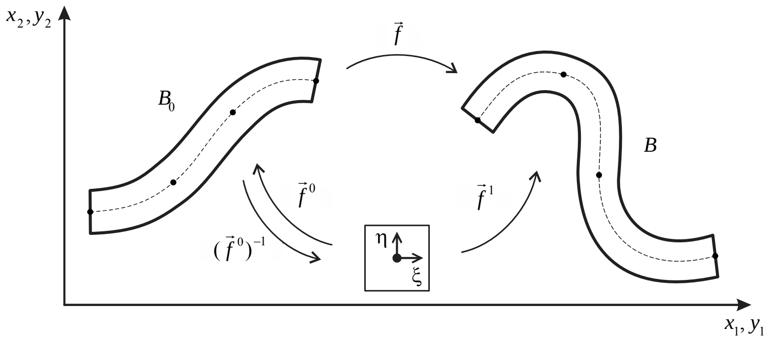

Fig. 2. Deformation mapping

As there is no relation between the cross section angle and the slope of the reference line, the frame kinematic can be regarded as Reissner's. It should be mentioned that the cross section dimensions are maintained the same during motion, thus, to avoid volumetric locking, the constitutive equation is relaxed in order to exclude transverse expansions.

Kinematical constraints due to sliding connections

To develop the friction force it is required first to describe how the constraint equations for the sliding connections are defined, particularly concerning the curvilinear position, which is a new variable introduced in the equations of motion, and at which this force will act. Here we summarize the description of the connections as a prismatic or a cylindrical joint. More details can be obtained in [11].

Sliding connections are the ones that constrain relative translations between parts of the body. Fig. 3 illustrates both joints and their plane representation. In either case, a sliding node, at which the joint exists, is constrained to move over a trajectory comprised of path elements. The difference between the prismatic and the cylindrical joint is the relative rotation, which is allowed only by the last one.

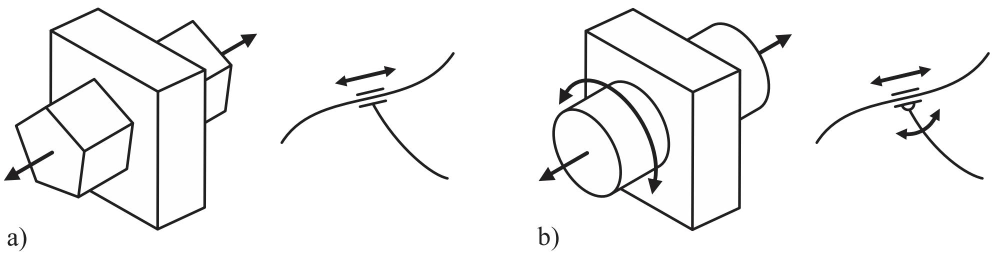

Fig. 3. Sliding connections and its plane representation: a) prismatic and b) cylindrical joints

Fig. 4 depicts the case of a prismatic joint, belonging to node $\hat{P}$, and its path contact point $\overline{P}$. The connection is free to move along the path $s(\xi)$ defined by path finite elements, which, although not used in this work, may have an arbitrary roughness profile $\vec{r}(s)$. The notation $(\overline{\bullet})$ is used to identify variables related to path elements and $(\hat{\bullet})$ is used for sliding elements. The new variable $s_P = s(\xi_P)$ that defines the curvilinear position and the cross section orientation of the path point is also illustrated.

The constraint equations, $\vec{c}$, can be written for both types of joints as a single expression:

$$c_i = \hat{Y}_i^P - \phi_\ell(\xi_P)\bar{Y}_i^\ell - \Delta\theta_P^0\delta_{i3} - r_i(s_P)(1-\delta_{(i)3}) = 0_i \tag{7}$$

where: i is the direction ($i = 1,2,3$ for prismatic joints and $i = 1,2$ for cylindrical joints); δ_{ij} is the Kronecker delta; $\Delta\theta_P^0 = \hat{\theta}_P^0 - \bar{\theta}_P^0$ is the difference of cross sections orientations at the initial configuration, which must be constant during the sliding process of a prismatic joint to maintain a fixed relative angle; and the components of the roughness profile, obtained by its height function $\| \vec{r}(s) \|$, are given by:

$$\begin{aligned} r_1(s_P) &= \|\vec{r}(s_P)\| \cos\left[\phi_\ell(\xi_P)\bar{\theta}_\ell\right] \\ r_2(s_P) &= \|\vec{r}(s_P)\| \sin\left[\phi_\ell(\xi_P)\bar{\theta}_\ell\right] \end{aligned} \tag{8}$$

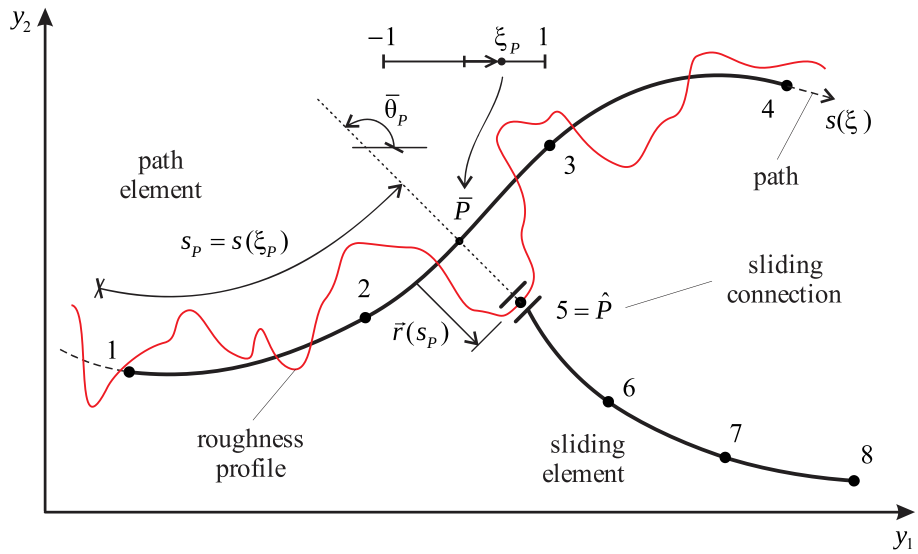

Fig. 4. Sliding connection over an arbitrary path (depicted for a prismatic joint)

It is noteworthy that the curvilinear variable $s(\xi)$ represents an arch-length function defined by the non-dimensional coordinate ξ and the path element coordinates.

Unconstrained equations of motion

Using the Law of Conservation of Energy, the dynamical equilibrium of a conservative system is obtained by its total energy Π_0 as:

$$\Pi_0 = \Pi - \mathcal{Q} \tag{9}$$

where $\mathcal{Q}$ represents the dissipation of a 'larger' system of total energy Π. Eq. (9) can be rewritten as:

$$\Pi = \Pi_0 + \mathcal{Q} \tag{10}$$

or, making explicit the energy parcels of the new larger conservative system:

$$\Pi = \mathcal{U} - \mathcal{P} + \mathcal{K} + \mathcal{Q} \tag{11}$$

where $\mathcal{U}$ is the stored elastic strain energy, $\mathcal{P}$ is the potential of conservative external forces and $\mathcal{K}$ is the kinetic energy of the body.

Following Lanczos and others [15–17], it is not always possible to write down closed expressions for dissipative parcels but only its infinitesimal change. Thus, the equations of motion are stated from the variation of the energies present in eq. (11), which is understood as the Principle of Stationary Total Energy:

$$\delta\Pi = \delta\mathcal{U} - \delta\mathcal{P} + \delta\mathcal{K} + \delta\mathcal{Q} = 0 \tag{12}$$

in which the symbol δ means variation.

The total energy can be stated by writing the known expressions of the energies in eq. (11) as function of the current configuration nodal parameters of the discretized body, grouped in the vector $\vec{Y}$, as:

$$\Pi(\vec{Y}) = \int_{V_0} u(\mathbf{E}(\vec{Y}))dV_0 - \vec{F}\cdot\vec{Y} - \int_{s_0} \vec{q}\cdot\vec{y}\,ds_0 + \frac{1}{2}\int_{V_0} \rho_0 \dot{\vec{y}}\cdot\dot{\vec{y}}\,dV_0 + \mathcal{Q}(\vec{Y}) \tag{13}$$

where the specific strain energy u depends on the strain state $\mathbf{E}$ of the body, eq. (6), which is function of the nodal parameters $\vec{Y}$, as defined by the gradient of the deformation function in eq. (4).

As mentioned before, the Saint-Venant-Kirchhoff constitutive relation is employed due to its simplicity and good representation of large displacements on solids that remain in the small to moderate strain regimen, which comprehends the majority of the usual applications in engineering. For the plane frame utilized, its specific energy is given as:

$$u = \frac{\mathbb{E}}{2}\left(E_{11}^2 + E_{22}^2\right) + \mathbb{G}\left(E_{12}^2 + E_{21}^2\right) \tag{14}$$

where $\mathbb{E}$ is the longitudinal elastic parameter that approaches the Young modulus for small strains. The shear elastic modulus is $\mathbb{G} = \mathbb{E}/[2(1+\nu)]$, being ν a constant that reproduces the Poisson ratio for small strains. The second Piola-Kirchhoff stress tensor is easily obtained by the energy conjugacy property as:

$$\mathbf{S} = \frac{\partial u}{\partial \mathbf{E}} \tag{15}$$

Still in eq. (13), $\vec{F}$ and $\vec{q}$ are the concentrated and distributed conservative external loading, respectively. The initial length of the frame reference line is s_0. The material mass density in the initial configuration, of volume V_0, is ρ_0. The material points' velocity is denoted using the over-dot as $\dot{\vec{y}}$. External damping dissipation, proportional to the velocity in its differential form (Rayleigh damping), is introduced as:

$$\frac{\partial\mathcal{Q}}{\partial\vec{y}}\cdot\delta\vec{y} = \int_{V_0} c_\rho \rho_0 \dot{\vec{y}}\cdot\delta\vec{y}\,dV_0 \tag{16}$$

in which c_ρ is a proportionality constant.

The equations of motion (geometric nonlinear dynamical equilibrium) are obtained by the development of the variations in eq. (13). In a compact form, the equilibrium can be written as:

$$\vec{F}^{\text{int}} - \vec{F} + \mathbf{M}\cdot\ddot{\vec{Y}} + \mathbf{D}\cdot\dot{\vec{Y}} = \vec{0} \tag{17}$$

where: $\vec{F}^{\text{int}} = Grad(\mathcal{U})$ is the internal force vector; $\vec{F}$ collects all the external loads; $\mathbf{M}$ is a constant mass matrix; $\mathbf{D} = c_\rho\mathbf{M}$ is the external damping matrix; and $\dot{\vec{Y}}$ and $\ddot{\vec{Y}}$ are the velocity and acceleration vectors of the nodal parameters. More details about the development of the variations of eq. (13) can be obtained in [10,11].

Constrained equations of motion

The dynamical equilibrium stated by eq. (17) is called unconstrained since no restraints, such as the ones from the sliding connections, are considered. The literature presents several consolidated methodologies to impose constraints such as in [15,18] on mechanical and structural applications or in [19–21] which deal with general optimization problems. Here, we employ the well-known Lagrange multiplier method along with the Principle of Stationary Total Energy to impose the sliding restrictions. In what regards the later introduction of friction dissipation, the multipliers are of great value since in Mechanics they might be understood as the contact forces between bodies, an essential information for the friction model.

The Principle of Stationary Total Energy is extended for the case of holonomic constraints by modifying the total energy through the introduction of a new potential $\mathcal{C}$, referred as the constraint potential, as:

$$\Pi = \mathcal{U} - \mathcal{P} + \mathcal{K} + \mathcal{Q} + \mathcal{C} \tag{18}$$

When using Lagrange multipliers the expression of the new potential is simply given by:

$$\mathcal{C} = \vec{\lambda} \cdot \vec{c} \tag{19}$$

where $\vec{\lambda}$ represents the vector of multipliers, which are new variables of the system. Eq. (19) indicates the presence of a multiplier for each constraint equation in $\vec{c}$. It is worth mentioning that the constraint potential is null at the solution, therefore, the total energy is not altered.

Knowing the expression of $\mathcal{C}$, the first variation of the constrained energy, eq. (18), is:

$$\delta\Pi = \delta\mathcal{U} - \delta\mathcal{P} + \delta\mathcal{K} + \delta\mathcal{Q} + \delta\mathcal{C} = 0 \tag{20}$$

which, neglecting friction, can be developed in a similar fashion as the unconstrained case leading to the constrained equations of motion (constrained geometric nonlinear dynamical equilibrium), expressed in a compact form as:

$$\vec{F}^{\mathrm{int}} - \vec{F} + \mathbf{M} \cdot \ddot{\vec{\Upsilon}} + \mathbf{D} \cdot \dot{\vec{\Upsilon}} + \vec{F}^{\mathrm{c}} = \vec{0} \tag{21}$$

in which $\vec{F}^{\mathrm{c}}$ represents the restriction forces arriving from the constraint potential. As the multipliers are new variables, the variation of $\mathcal{C}$ is organized in the following force vector, which separates the parameters $\vec{\Upsilon}$ (including s_P) and the multipliers:

$$\delta\mathcal{C} = \delta\vec{\Upsilon} \cdot \nabla\vec{c} \cdot \vec{\lambda} + \delta\vec{\lambda} \cdot \vec{c} = \left\{ \delta\vec{\Upsilon} \quad \delta\vec{\lambda} \right\} \cdot \left\{ \begin{matrix} \nabla\vec{c} \cdot \vec{\lambda} \\ \vec{c} \end{matrix} \right\} = \left\{ \delta\vec{\Upsilon} \quad \delta\vec{\lambda} \right\} \cdot \vec{F}^{\mathrm{c}} \tag{22}$$

where the tensor $\nabla\vec{c}$ represents the Jacobian matrix of the constraint vector. In order to shorten this presentation, the derivatives of the constraint equation for the sliding connections, eq. (7), can be found in reference [11].

Friction force on the sliding connection

The friction force is included in the system directly in the Principle of Stationary Total Energy as a dissipative potential. As mentioned previously, dissipative potentials are introduced in their differential form since closed expressions might be unknown, as is the case for the dissipated friction energy $\mathcal{Q}_{\mathrm{f}}$. However, the variation of this potential can be written as the work done by the friction force $\vec{F}^{\mathrm{f}}$ on its displacement trajectory $\vec{d}$ as:

$$\delta\mathcal{Q}_{\mathrm{f}} = \vec{F}^{\mathrm{f}} \cdot \delta\vec{d} \tag{23}$$

To develop eq. (23), parameters that describes the force displacement must be chosen. For that, the coordinates of the sliding node and its path contact point could be picked. However, since in the previous formulation the curvilinear position s_P is already used as an intrinsic variable, the displacement along the trajectory is simply the scalar expression $d = s_p - s_P^0$, being s_P^0 an arbitrary initial value, and its variation is $\delta d = \delta s_p$. As the friction force acts tangentially to the trajectory, with its value given by F_f, the dissipative parcel is introduced directly in the curvilinear position as:

$$\delta \mathcal{Q}_\mathrm{f} = F_\mathrm{f}\, \delta s_P \tag{24}$$

To organize the equations of motion system, we make $\vec{\Lambda}^\mathrm{f} = \{F_\mathrm{f}\}$, the previous equation is rewritten as:

$$\delta \mathcal{Q}_\mathrm{f} = \{\delta s_P\} \cdot \vec{\Lambda}^\mathrm{f} \tag{25}$$

Considering the correspondence of the friction force vector $\vec{\Lambda}^\mathrm{f}$ to the system variables, the equations of motion are restated to include frictional dissipation as:

$$\vec{F}^\mathrm{int} - \vec{F} + \mathbf{M} \cdot \ddot{\vec{Y}} + \mathbf{D} \cdot \dot{\vec{Y}} + \vec{F}^\mathrm{c} + \vec{\Lambda}^\mathrm{f} = \vec{0} \tag{26}$$

Improved friction model

From the manner that the friction force was introduced in the formulation any expression can be readily applied without changing the equilibrium equation. In this work, we employ the Coulomb model considering the Stribeck effect and viscous friction. Fig. 5 shows the overall behaviour of the friction force with the relative velocity among bodies. This model considers the stick-slip effect, which is the difference between the friction force at rest (static friction) and at motion (kinetic friction), by the Stribeck curve, using the most usual expression proposed by Bo e Pavelescu [22]. A linear model represents the viscous friction, which occurs if lubricant layers are present on the surfaces.

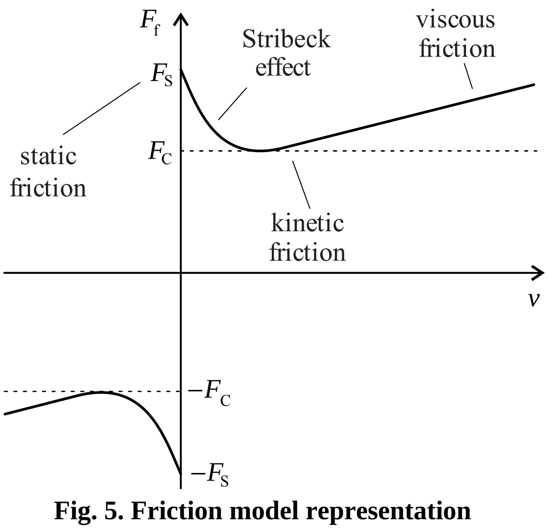

Fig. 5. Friction model representation

The mathematical expression for the friction force due this model is written as:

$$F_f = \begin{cases} \left[F_C + (F_S - F_C) e^{-(|v|/v_\sigma)^{\delta_\sigma}} \right] \mathrm{sgn}(v) + \eta v & \text{if} \quad v \neq 0 \\ \min(F_S,\, F_R)\, \mathrm{sgn}(F_R) & \text{if} \quad v = 0 \end{cases} \tag{27}$$

with the static and kinetic friction forces, respectively, given by:

$$F_S = \mu_s F_N \qquad \text{and} \qquad F_C = \mu_k F_N \tag{28}$$

where, μ_s and μ_k are, respectively, the static and kinetic friction coefficients and F_N the absolute value of the contact force normal to the trajectory at the joint contact point. In addition, η is the viscous friction coefficient and $v = \dot{s}_P$ is the joint relative velocity tangential to the path (directly obtained from the curvilinear position). The Stribeck parameters are its decay velocity v_σ and power δ_σ. The sign function is represented by $\mathrm{sgn}(\bullet)$.

For null relative velocity, second condition in eq. (27), the tangential resultant force F_R acting on the connection is required for comparison with the static friction value. This evaluation verifies if there is tendency of motion in case the resultant force is greater than the static friction force, or not, otherwise. However, in the transition from motion to rest, the shift from one force to another is done abruptly using their smallest value, which, as concern numerical simulations, may create instabilities in the system solution and the need to use very small time steps.

For this reason, a linear interpolation between the values of the static friction force and the resultant force is proposed for the stabilization of the friction force response when there is a range $[-v_0, v_0]$ of quasi-null velocities, as depicted in Fig. 6.

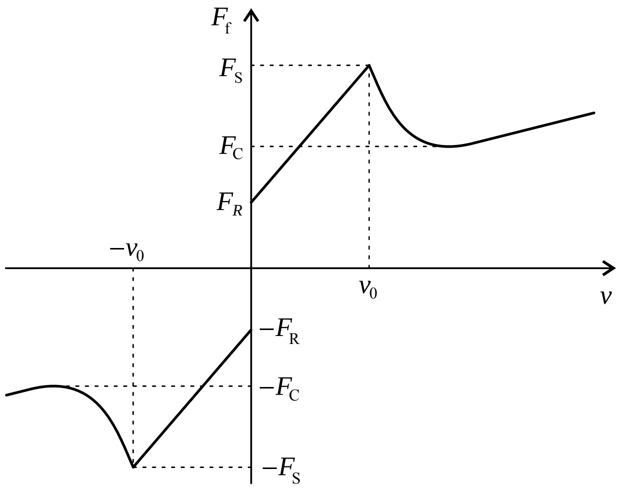

Fig. 6. Improved friction model

The improved friction model is written as:

$$F_f = \begin{cases} \left[F_C + (F_S - F_C) e^{-(|v|/v_\sigma)^{\delta_\sigma}} \right] \mathrm{sgn}(v) + \eta v & \text{if} \quad |v| > |v_0| \\ -F_S \,\mathrm{sgn}(F_R) & \text{if} \quad |v| \leq |v_0| \quad \text{and} \quad |F_R| \geq F_S \\ \dfrac{F_S - |F_R|}{|v_0|} v + F_R & \text{if} \quad |v| \leq |v_0| \quad \text{and} \quad |F_R| < F_S \end{cases} \tag{29}$$

where v_0 is the quasi-null speed limit. One should note that F_C and F_S are always positive since they are obtained from the absolute value of the normal force, eq. (28), thus, the sign of the friction force in eq. (29) depends on the values and signs of the relative velocity and resultant force.

In the proposed approach, F_R is not a constant value, but depends upon the system own force state at a given time instant, which can even be null, if applicable. Therefore, the system response can be stabilized by means of a smooth transition from the motion state to rest state and vice versa. In addition, by taking into account the resulting force, the proposed improved friction model is capable to represent residual displacements of the sliding connection.

It should be noted that the quasi-null speed limit value v_0 depends on the adopted time step, or, inversely, the chosen time step has to be able to represent the movement when in the quasi-null velocity interval. For better convergence of the iterative solution method, the recommended value of the limit velocity should be close to the relative stop speed of the bodies but not too small to allow the smooth transition among forces at rest.

Known the coefficients of the model, which depends on the materials that make the sliding connection and its path, the forces required to calculate the friction force have to be related to the variables that describe the joint. The normal force vector $\vec{F}^N$ is found from the component of the Lagrange multipliers vector due to the translational constraints, $\vec{\lambda} = \{\lambda_1, \lambda_2\}$, at the normal direction of the path at the contact point, defined by the normal vector $\vec{\bar{N}}^P$, as:

$$\vec{F}^N = \frac{\vec{\lambda} \cdot \vec{\bar{N}}^P}{\left\| \vec{\bar{N}}^P \right\|} \frac{\vec{\bar{N}}^P}{\left\| \vec{\bar{N}}^P \right\|} \tag{30}$$

and its absolute value, actually used in the calculation, is:

$$F_\mathrm{N} = \left\| \vec{F}^N \right\| = \frac{\left| \vec{\lambda} \cdot \vec{\bar{N}}^P \right|}{\left\| \vec{\bar{N}}^P \right\|} \tag{31}$$

In the plane case, the components of the normal vector are obtained from the tangent vector of the path finite element at the contact point, $\bar{T}_i^P = \phi_{\ell,\xi}(\xi_P)\bar{Y}_i^\ell$ $(i = 1,2)$, as $\bar{N}_1^P = -\bar{T}_2^P$ and $\bar{N}_2^P = \bar{T}_1^P$.

The resultant force, equal to the inertial force at the sliding node, is obtained directly from the equilibrium equation (26), considering only the sliding node degrees of freedom (positions and curvilinear variable), as:

$$\vec{F}^R = \vec{F} - \vec{F}^{\mathrm{int}} - \vec{F}^{\mathrm{c}} \tag{32}$$

or, as to identify the terms referred to the degrees of freedom:

$$\begin{Bmatrix} F^R_{\bar{Y}_1^P} \\ F^R_{\bar{Y}_2^P} \\ F^R_{s_P} \end{Bmatrix} = \begin{Bmatrix} F_{\bar{Y}_1^P} \\ F_{\bar{Y}_2^P} \\ F_{s_P} \end{Bmatrix} - \begin{Bmatrix} F^{\mathrm{int}}_{\bar{Y}_1^P} \\ F^{\mathrm{int}}_{\bar{Y}_2^P} \\ 0 \end{Bmatrix} - \begin{Bmatrix} F^{\mathrm{c}}_{\bar{Y}_1^P} \\ F^{\mathrm{c}}_{\bar{Y}_2^P} \\ F^{\mathrm{c}}_{s_P} \end{Bmatrix} \tag{33}$$

where $\vec{F}$ represents all the external loads, $\vec{F}^{\mathrm{int}}$ the internal force of the sliding element and $\vec{F}^{\mathrm{c}}$ the connection constraint force. Subscripts $\bar{Y}_1^P$, $\bar{Y}_2^P$ and s_P refer to the sliding node position degrees of freedom and the curvilinear position, respectively. In the definition of eq.

(32), being a quasi-null velocity case, the velocity-proportional external damping was neglected. The friction force is also not present since its value is already considered indirectly through the constraint force at the curvilinear position direction. As the tangential value of the resultant force F_R is required, the tangent vector is used to decompose the Cartesian terms as:

$$F_R = \frac{\left(F_{\bar{Y}_1^P} - F_{\bar{Y}_1^P}^{\text{int}} - F_{\bar{Y}_1^P}^{\text{c}}\right)\bar{T}_1^P + \left(F_{\bar{Y}_2^P} - F_{\bar{Y}_2^P}^{\text{int}} - F_{\bar{Y}_2^P}^{\text{c}}\right)\bar{T}_2^P}{\left\|\vec{\bar{T}}^P\right\|} + F_{s_P} - F_{s_P}^{\text{c}} \tag{34}$$

As expected from the physical significance of the multipliers as contact forces, we have $F_{\bar{Y}_1^P}^{\text{c}} = \lambda_1$ and $F_{\bar{Y}_2^P}^{\text{c}} = \lambda_2$. This result can be obtained by developing the constraint force given in eq. (22) for the constraint equation in (7).

Time integration and nonlinear system solution procedure

For the time discretization and nonlinear system solution, the equations of motion (26) are written for a specific time instant as:

$$\vec{g}\left(\vec{Y}_{t+1}, \vec{\lambda}_{t+1}\right) = \vec{F}_{t+1}^{\text{int}} - \vec{F}_{t+1} + \mathbf{M} \cdot \ddot{\vec{Y}}_{t+1} + \mathbf{D} \cdot \dot{\vec{Y}}_{t+1} + \vec{F}_{t+1}^{\text{c}} + \vec{\Lambda}_{t+1}^{\text{f}} = \vec{0} \tag{35}$$

where $\vec{g}$ is the residual of the Newton method (or mechanical unbalanced vector), null when $\vec{Y}_{t+1}$ and $\vec{\lambda}_{t+1}$ are a solution of the system of equations. One can note that $\vec{\lambda}_{t+1}$ only appear in the terms $\vec{F}_{t+1}^{\text{c}}$ and $\vec{\Lambda}_{t+1}^{\text{f}}$.

Since the description of the solid is made by a total Lagrangian approach, the inertial force is obtained using a constant mass matrix which allows the adoption of the Newmark approximations for the material velocity and acceleration vectors, see, for instance, the discussion in [23–25]. Those approximations for a time step Δt, with its usual parameters β and γ, are given by:

$$\vec{Y}_{t+1} = \vec{Y}_t + \Delta t \dot{\vec{Y}}_t + \Delta t^2 \left[\left(\frac{1}{2} - \beta\right)\ddot{\vec{Y}}_t + \beta \ddot{\vec{Y}}_{t+1}\right] \tag{36}$$

$$\dot{\vec{Y}}_{t+1} = \dot{\vec{Y}}_t + \Delta t (1-\gamma)\ddot{\vec{Y}}_t + \gamma \Delta t \ddot{\vec{Y}}_{t+1} \tag{37}$$

Substituting both previous expressions in eq. (35) we arrive at:

$$\begin{aligned} \vec{g}\left(\vec{Y}_{t+1}, \vec{\lambda}_{t+1}\right) = \vec{F}_{t+1}^{\text{int}} - \vec{F}_{t+1} + \left(\frac{\mathbf{M}}{\beta \Delta t^2} + \frac{\gamma \mathbf{D}}{\beta \Delta t}\right) \cdot \vec{Y}_{t+1} + \vec{F}_{t+1}^{\text{c}} \\ + \vec{\Lambda}_{t+1}^{\text{f}} - \mathbf{M} \cdot \vec{T}_t + \mathbf{D} \cdot \vec{R}_t - \gamma \Delta t \mathbf{D} \cdot \vec{T}_t = \vec{0} \end{aligned} \tag{38}$$

in which $\vec{T}_t$ and $\vec{R}_t$ represents the dynamical contribution of the previous time step as:

$$\vec{T}_t = \frac{\vec{Y}_t}{\beta \Delta t^2} + \frac{\dot{\vec{Y}}_t}{\beta \Delta t} + \left(\frac{1}{2\beta} - 1\right)\ddot{\vec{Y}}_t \qquad \text{and} \qquad \vec{R}_t = \dot{\vec{Y}}_t + \Delta t (1-\gamma)\ddot{\vec{Y}}_t \tag{39}$$

For the friction force calculation, eq. (29), the Newmark expressions are employed to approximate the tangential velocity $v = \dot{s}_P$. Consequently, this force is entirely defined in a time step $t+1$ by the Lagrange multipliers, curvilinear position and current path finite element nodal positions.

Eq. (38) is clearly nonlinear for the variables $\{\vec{Y}_{t+1}, \vec{\lambda}_{t+1}\}$, thus, a usual first order Taylor expansion can be employed to obtain the Newton method as:

$$\begin{Bmatrix} \Delta \vec{Y}_{t+1} \\ \Delta \vec{\lambda}_{t+1} \end{Bmatrix} = -\left(\mathbf{H}_{t+1}\right)^{-1} \cdot \vec{g}\left(\vec{Y}^{0}_{t+1}, \vec{\lambda}^{0}_{t+1}\right) \tag{40}$$

in which, the correction $\{\Delta \vec{Y}_{t+1}, \Delta \vec{\lambda}_{t+1}\}$ is obtained from the trial solution $\{\vec{Y}^{0}_{t+1}, \vec{\lambda}^{0}_{t+1}\}$ and the Hessian matrix given by:

$$\mathbf{H}_{t+1} = \nabla \vec{g}_{t+1} = \mathbf{H}^{\mathbf{e}}_{t+1} + \mathbf{H}^{\mathbf{c}}_{t+1} \tag{41}$$

The Hessian related to the energy potentials due to individual finite elements is called $\mathbf{H}^{\mathbf{e}}$ and its expressions can be found in [10,11]. The Hessian matrix due the constraint potential of the sliding connections is written as:

$$\mathbf{H}^{\mathrm{c}} = \frac{\partial \vec{F}^{\mathrm{c}}}{\partial\{\vec{Y}, \vec{\lambda}\}} = \begin{bmatrix} \vec{\lambda} \cdot \nabla(\nabla \vec{c}) & \nabla \vec{c} \\ (\nabla \vec{c})^{t} & \mathbf{0} \end{bmatrix} \tag{42}$$

where, $\nabla(\nabla \vec{c})$ is a third order tensor that can be understood as the set of Hessian matrices due to each constraint equation c_i, and $\mathbf{0}$ is the null matrix.

It must be stressed that, however achieved a value for s_P in the solution process, it is not sufficient to update $\vec{F}^{\mathrm{c}}$ and the Hessian matrix as the function $\xi_P = \xi(s_P)$ is not explicitly written. The solution of this stage is done by adopting a least square method to find the non-dimensional coordinate from the converged values of the path element and the sliding node as described in detail by [11]. Given the numerical value of the non-dimensional variable in the dimensionless space, the transitions among path elements is straightforward when its value exceeds the space domain.

Examples

Some examples are presented to show the capabilities of the proposed formulation regarding the correct description of the friction force and its structural effects. In all simulations, the Newmark parameters for the average acceleration in the time step were adopted, $\beta = 0.25$ and $\gamma = 0.50$, which do not introduce numerical damping in the solution.

Axial vibration with friction dissipation

To validate the improved friction model we employ the structure depicted in Fig. 7 a) which consists of a bar with length $L = 1.0\,\mathrm{m}$ submitted to an initial displacement $d = 1.0\,\mathrm{mm}$ at its left extremity (proportionally distributed over its extension). A cylindrical joint exists at the same end, which is free to move over a finite element with locked degrees of freedom to simulate a rigid support. A vertical force $P = 2000\,\mathrm{N}$ is applied to manifest frictional effects on the connection.

Discretizing the bar with one two-noded (linear) frame element results the equivalent mass-spring system shown in Fig. 7 b). Adopting a squared cross-section with $b_0 = h_0 = 0.1\,\mathrm{m}$ and Young modulus $\mathbb{E} = 2 \cdot 10^{8}\,\mathrm{Pa}$, the axial spring stiffness is $k = \mathbb{E} b_0 h_0 / L = 2 \cdot 10^{6}\,\mathrm{N/m}$. The shear modulus is half the value of the Young modulus. The equivalent system mass $m = 5.066\,\text{kg}$ is lumped at the joint node. Knowing all the system parameters, the mass-spring natural frequency is given by $\omega_n = \sqrt{k/m} = 628.38\,\text{rad/s}$, and its oscillation period is $T_n = 2\pi/\omega_n = 0.01\,\text{s}$. For this reason, the adopted time increment is $\Delta t = 10^{-4}\,\text{s}$.

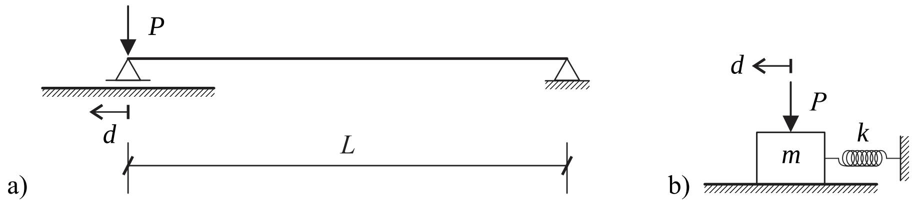

Fig. 7. Geometries of the systems: a) continuous and b) mass-spring

The sliding connection displacement for the frictionless case is shown in Fig. 8 where the harmonic oscillation with expected period and amplitude values are reached. Also in Fig. 8, two cases of friction are simulated: one with dry friction only and the other that adds the viscous friction term. Adopted dry friction parameters are $\mu_s = 0.05$, $\mu_k = 0.03$, $v_\sigma = 0.1\,\text{m/s}$ and $\delta_\sigma = 2$, for the viscous case $\eta = 100\,\text{Ns/m}$. The quasi-null speed limit was chosen as $v_0 = 2 \cdot 10^{-3}\,\text{m/s}$. This mass-spring system subjected only to Coulomb kinetic friction has analytical solution presented in [26]. In spite of the reference solution have been proposed for a simpler case, one can verify in a similar manner that the friction dissipation did not altered the system oscillation period. Moreover, the decay envelope for the dry case is liner whereas when adding the viscous term the envelope changed to an exponential tendency, as is expected from its similarity to a one degree of freedom mass-spring-damper system.

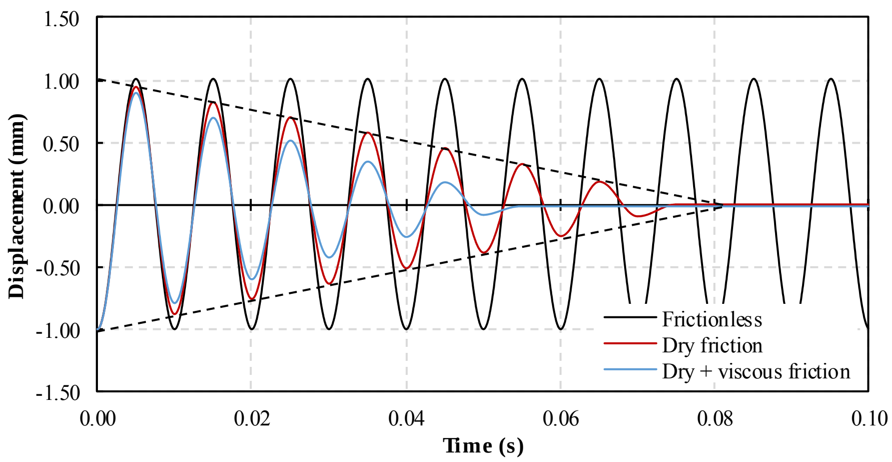

Fig. 8. Displacement of the equivalent mass-spring system

With the proposed improved friction model, the residual displacement is correctly captured as illustrated in Fig. 9. This displacement occurs when the spring restitution force, i.e., its internal force, and the friction force become balanced outside the bar undeformed configuration. This effect can only be properly represented since the resultant force is calculated in the friction model.

Given the existence of residual displacements, the friction force also has a residual value as shown in Fig. 10. For the case with viscous friction the force value at rest is $-30.93\,\text{N}$. For this small displacement analysis, from the spring stiffness one can obtain the residual displacement as $F_f / k = -1.5465 \cdot 10^{-2}$ mm, which is exactly the simulation value in Fig. 9.

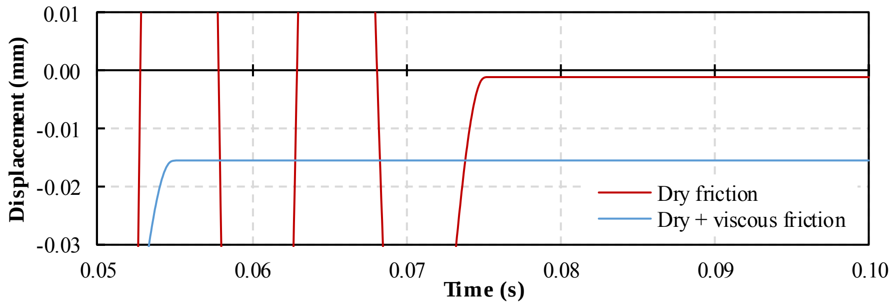

Fig. 9. Residual displacement for the equivalent mass-spring system

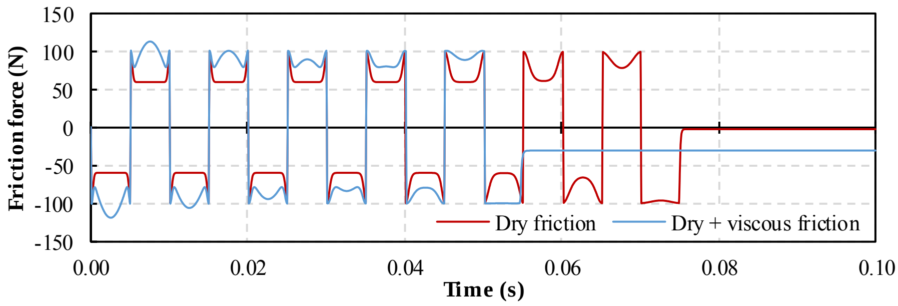

Fig. 10. Friction force for the equivalent mass-spring system

The evolution of the strain energy (S.E.) and the kinetic energy (K.E.) are also interesting parameters to be observed (Fig. 11). For the frictionless case the sum of those energies is constant throughout the analysis. We highlight that, although there is an external load applied, no energy is associated to it since there is no displacement in its direction. When friction is introduced in the system the energies sum decay with time, faster for the viscous friction case than to the dry one as is expected from the higher friction values obtained (Fig. 10). Due the existence of residual displacements, there is also a residual energy as presented in the detail of Fig. 11 in log scale. The rest energies sum of the viscous friction case is obtained in the simulation equal to $0.2392\,\text{mJ}$. The same value can be found from the spring strain energy $kd^2/2$, being d the residual displacement, revealing that its residual energy value is due only to the bar deformation.

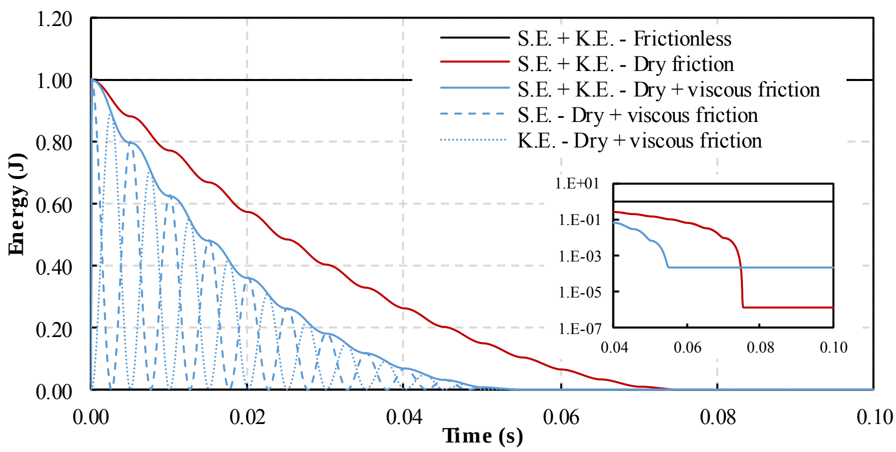

Fig. 11. Energy time history of the equivalent mass-spring system

Increasing the spatial discretization to 10 cubic finite elements, and adopting a mass density of $\rho_0 = 1250\,\text{kg/m}^3$, one achieves the same oscillation period for the mass-spring system. To analyse this discretized continuous system, all previous parameters were kept but the quasi-null speed limit $v_0 = 3\cdot 10^{-2}\,\text{m/s}$ and the time step $\Delta t = 1.25\cdot 10^{-5}\,\text{s}$. The time increment was chosen to allow a good representation of the passage of the axial displacement wave in the domain of each finite element. This wave has velocity $c = \sqrt{\mathbb{E} b_0 h_0 / \rho_0} = 4000\,\text{m/s}$. Fig. 12 shows the displacement results for both friction cases and the frictionless one. As expected, the oscillation period, amplitude and decay type is similar to the equivalent system.

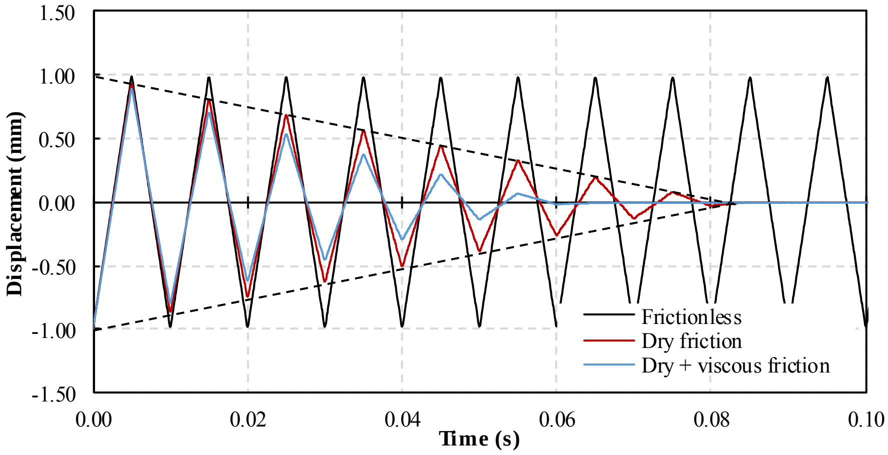

Fig. 12. Sliding connection displacement for the discretized continuous system

The improved friction model was able to represent the residual displacement of the sliding connection for this continuous system as well (Fig. 13). However, due to the continuity of the bar and the only source of dissipation to be due to the joint friction, the remainder of the bar keeps vibrating as shown for the bar mid-point displacement history in Fig. 14. The last result shows the existence of a stationary wave of axial displacement between the extremity nodes, which are at rest, one due the boundary condition and the other due the friction force.

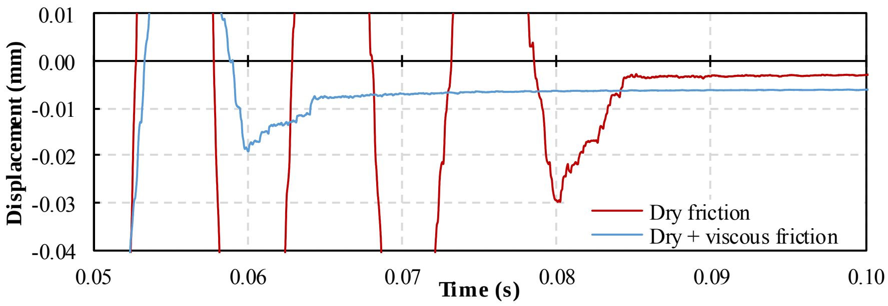

Fig. 13. Sliding connection residual displacement for the discretized continuous system

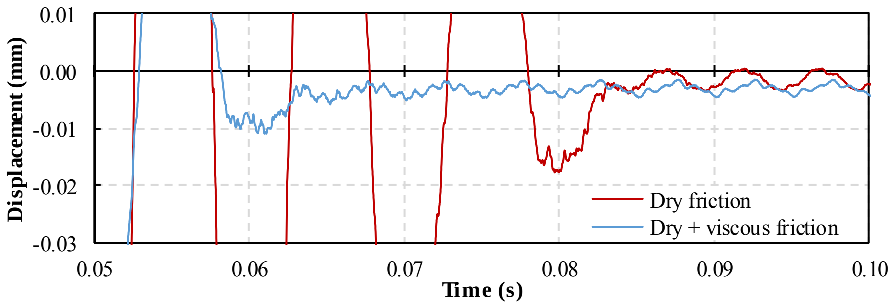

Fig. 14. Bar mid-point displacement for the discretized continuous system

Fig. 15 depicts the friction force time history for both cases. Oscillations on the value of the force during the perceptible displacements agree to the expected response of the discretized continuous system and occur due to higher vibrations modes that appear from the temporal and spatial resolutions adopted to represent properly the problem. We note that the employed model was able to capture the friction force reduction when the sliding connection is at rest and, due to the residual wave, its value shows a steady-state response that balances out the resultant force arriving from the rest of the body. Lastly, we present the energy time history for the continuous case for all the cases studied (Fig. 16). The energies sum decays in the presence of friction similarly to the mass-spring system.

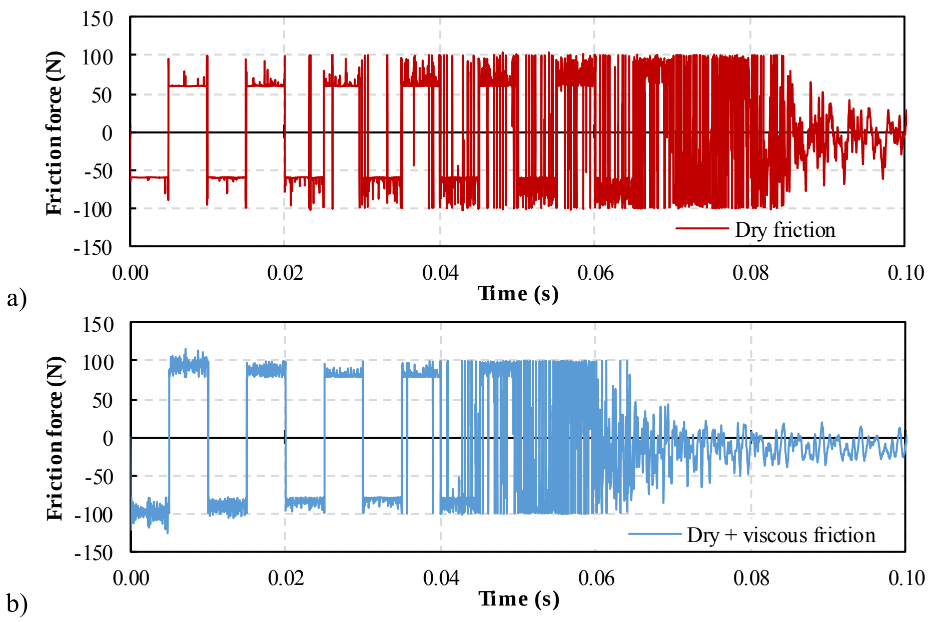

Fig. 15. Friction force for the discretized continuous system: a) dry friction and b) dry and viscous friction

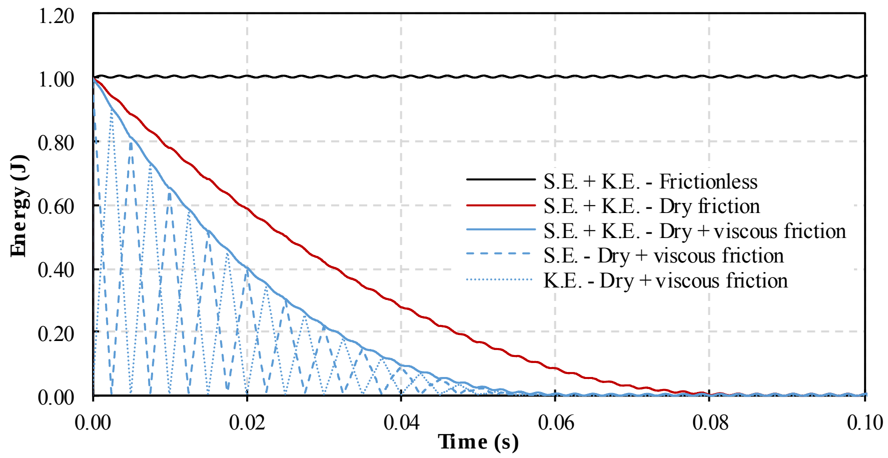

Fig. 16. Energy time history for the discretized continuous system

Driven mechanism with friction

For a more involved application, we propose the mechanism depicted in Fig. 17 subjected to a bending moment pulse in its crank. The moment M increases linearly from zero to $5\,k\mathrm{N.m}$ in $1\,\mathrm{s}$ and decreases to zero in another $1\,\mathrm{s}$ interval. To simulate a rigid crank its cross section is squared with $0.5\,\mathrm{m}$ side and its Young modulus is $2\cdot 10^{13}\,\mathrm{Pa}$. The other bars are flexible with squared cross section of $0.1\,\text{m}$ side and Young modulus equal $8\cdot10^{10}\,\text{Pa}$. For all bars, the mass density is $8000\,\text{kg/m}^3$ and the shear modulus is half the value of the Young modulus. The adopted time step is $0.01\,\text{s}$. Six cubic finite elements were used for the discretization. Friction parameters are: $\mu_s = 0.5$, $\mu_k = 0.3$, $v_\sigma = 0.001\,\text{m/s}$, $\delta_\sigma = 1$ and $v_0 = 1\cdot10^{-2}\,\text{m/s}$. No viscous friction in considered in the joint.

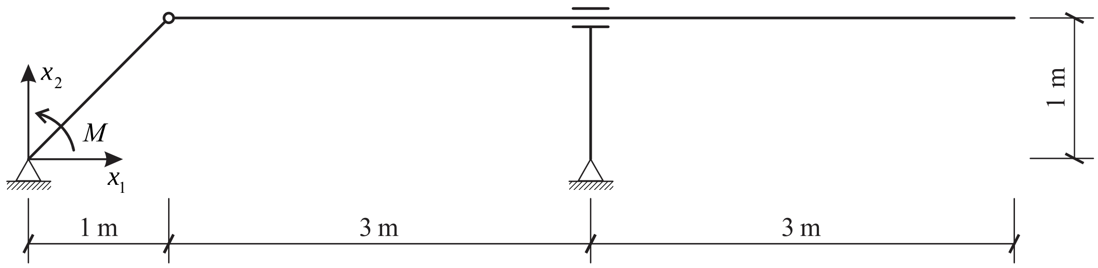

Fig. 17. Mechanism initial configuration

A prismatic joint is employed to connect the arm to a support bar. The sliding connection displacements are shown in Fig. 18 for cases with and without friction. The friction effect is perceived in the joint motion witch tends towards rest after the second rotation cycle of the mechanism, while the frictionless case presents free vibrations after the loading phase.

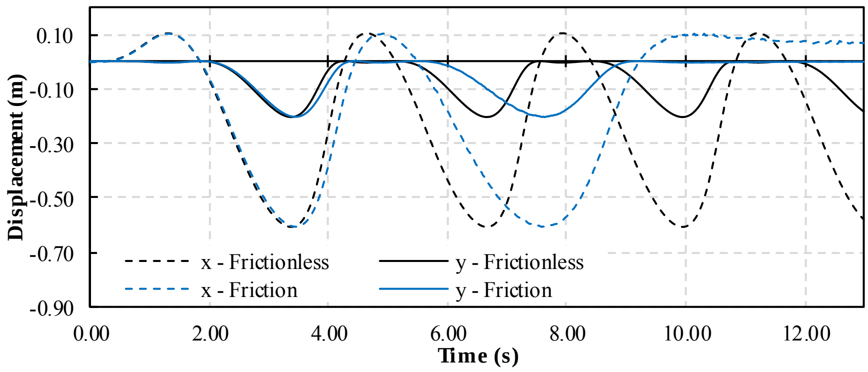

Fig. 18. Sliding connection displacements

The evolution of the curvilinear position (Fig. 19) displays similar results from the joint displacements. In Fig. 19 the position resting value is about 1.5 m from its arbitrary initial value, adopted as zero. Although expected, the curvilinear results are interesting since they can also be noted in the mechanism resting position as illustrated in Fig. 20 (the joint stops about ¼ of the arm length). The arm tip displacements (Fig. 21) also display the same behaviour.

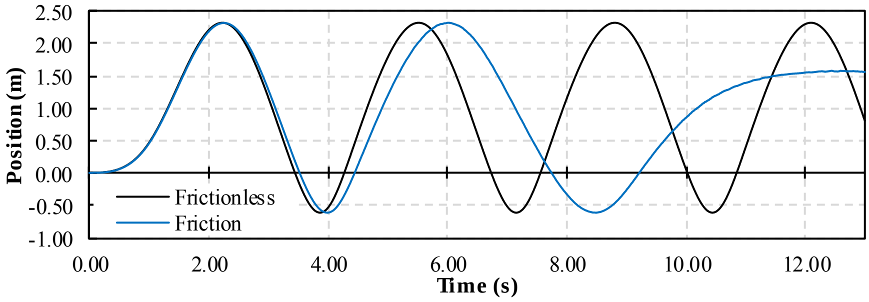

Fig. 19. Curvilinear position evolution

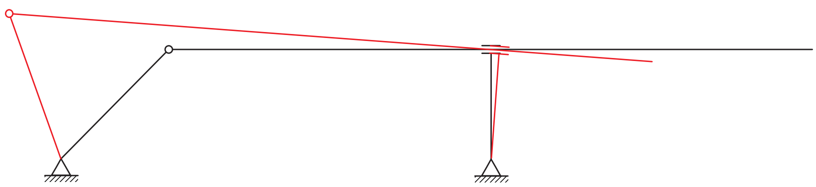

Fig. 20. Rest position (in red) of the mechanism when friction is present

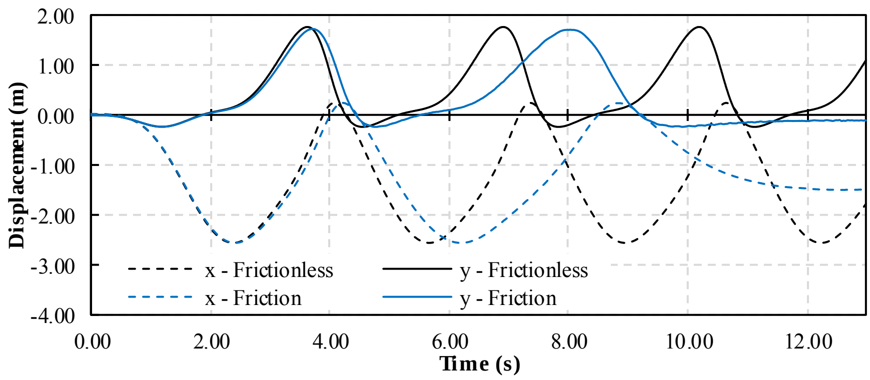

Fig. 21. Arm tip displacements

Conclusions

Friction dissipation was successfully introduced in sliding connections present in structures and mechanisms analysed by a total Lagrangian FEM formulation based on the positional description of the plane frame kinematic. Also, an improvement on the classic Coulomb friction model with Stribeck effect and viscous friction was proposed for a smoother description of the transition between motion and rest states of the joints. The proposed model was able to capture residual displacements of the body since the resultant force could be calculated properly and no instabilities were present in the friction force at null speed. Future studies intent to expand this formulation to 3D applications.

Acknowledgements

The authors would like to thank the São Paulo Research Foundation (FAPESP-2016/00622-0) for the financial support.

References

[1] Olsson H, Åström KJ, Canudas de Wit C, Gäfvert M, Lischinsky P. Friction Models and Friction Compensation. European Journal of Control 1998;4:176–95. doi:10.1016/S0947-3580(98)70113-X.

[2] Andersson S, Söderberg A, Björklund S. Friction models for sliding dry, boundary and mixed lubricated contacts. Tribology International 2007;40:580–7. doi:10.1016/j.triboint.2005.11.014.

[3] Marques F, Flores P, Pimenta Claro JC, Lankarani HM. A survey and comparison of several friction force models for dynamic analysis of multibody mechanical systems. Nonlinear Dynamics 2016;86:1407–43. doi:10.1007/s11071-016-2999-3.

[4] Threlfall DC. The inclusion of Coulomb friction in mechanisms programs with particular reference to DRAM au programme DRAM. Mechanism and Machine Theory 1978;13. doi:10.1016/0094-114X(78)90020-4.

[5] Karnopp D. Computer simulation of stick-slip friction in mechanical dynamic systems. Journal of Dynamic Systems, Measurement and Control, Transactions of the ASME 1985;107. doi:10.1115/1.3140698.

[6] Armstrong-Hélouvry B, Dupont P, De Wit CC. A survey of models, analysis tools and compensation methods for the control of machines with friction. Automatica 1994;30. doi:10.1016/0005-1098(94)90209-7.

[7] Ambrósio JAC. Impact of Rigid and Flexible Multibody Systems: Deformation Description and Contact Models. In: Schiehlen W, Valášek M, editors. Virtual Nonlinear Multibody Systems SE - 4, vol. 103, Dordrecht, Netherlands: Springer Netherlands; 2003, p. 57–81. doi:10.1007/978-94-010-0203-5_4.
[8] Wojewoda J, Stefański A, Wiercigroch M, Kapitaniak T. Hysteretic effects of dry friction: modelling and experimental studies. Philosophical Transactions of the Royal Society A: Mathematical, Physical and Engineering Sciences 2008;366. doi:10.1098/rsta.2007.2125.
[9] Awrejcewicz J, Grzelcyzk D, Pyryev Y. A novel dry friction modeling and its impact on differential equations computation and and Lyapunov exponents estimation. Journal of Vibroengineering 2008;10.
[10] Coda HB, Paccola RR. A total-Lagrangian position-based FEM applied to physical and geometrical nonlinear dynamics of plane frames including semi-rigid connections and progressive collapse. Finite Elements in Analysis and Design 2014;91:1–15.
[11] Siqueira TM, Coda HB. Total Lagrangian FEM formulation for nonlinear dynamics of sliding connections in viscoelastic plane structures and mechanisms. Finite Elements in Analysis and Design 2017;129:63–77. doi:10.1016/j.finel.2016.12.005.
[12] Bonet J, Wood RD, Mahaney J, Heywood P. Finite element analysis of air supported membrane structures. Computer Methods in Applied Mechanics and Engineering 2000;190:579–95. doi:10.1016/s0045-7825(99)00428-4.
[13] Coda HB. An exact FEM geometric non-linear analysis of frames based on position description. . IN: 17H INTERNATIONAL CONGRESS OF MECHANICAL ENGINEERING. 2003, São Paulo, São Paulo: ABCM; 2003.
[14] Ogden RW. Non-linear elastic deformations. Chichester: Ellis Horwood; 1984.
[15] Lanczos C. The variational principles of mechanics. New York: Dover Publications ; 1970.
[16] Gurtin ME, Fried E, Anand L. The Mechanics and Thermodynamics of Continua. New York: Cambridge University Press; 2010.
[17] Lemaitre J, Chaboche J-L. Mechanics of solid materials. Cambridge, Massachusets: Cambridge University Press; 1994.
[18] Géradin M, Cardona A. Flexible multibody dynamics: a finite element approach. Chichester: John Wiley & Sons; 2001.
[19] Nocedal J, Wright SJ. Numerical optimization. New York: Springer; 1999.
[20] Luenberger DG, Ye Y. Linear and nonlinear programming. 3rd ed. New York: Springer; 2008.
[21] Rao SS. Engineering optimization: theory and practice. 4th ed. New Jersey: John Wiley & Sons; 2009.
[22] Bo LC, Pavelescu D. The friction-speed relation and its influence on the critical velocity of stick-slip motion. Wear 1982;82. doi:10.1016/0043-1648(82)90223-X.
[23] Simo JC, Vu-Quoc L. On the dynamics in space of rods undergoing large motion - a geometrically exact approach. Computer Methods in Applied Mechanics and Engineering 1988;66:125–61. doi:10.1016/0045-7825(88)90073-4.
[24] Simo JC, Vu-Quoc L. On the dynamics of flexible beams under large overall motions — the plane case. II. Journal of Applied Mechanics-Transactions of the Asme 1986;53:855–63.
[25] Simo JC, Vu-Quoc L. On the dynamics of flexible beams under large overall motions — the plane case. I. Journal of Applied Mechanics-Transactions of the Asme 1986;53:849–54.
[26] Rao SS. Mechanical vibrations. 5th ed. Upper Saddle River, N.J: Pearson Prentice Hall; 2011.